We thank both anonymous reviewers for their constructive comments. We have addressed all of them in the following point-to-point rebuttal and we will incorporate the changes in the revised manuscript.
As comments by the reviewers have some common remarks, we have sorted each reviewer's comments and grouped those that have common themes.

We marked our responses in blue, in detail (we also uploaded this document as supplementary material, since we couldn't set font color in the interactive comment).

Reviewer 1, General comments: The paper uses InSAR to analyse surface deformation in an area of sinkholes formed due to salt mining in Solotvyno (Ukraine). The major results of the paper are: 1. two velocity maps and time series of LOS displacements, one in the ascending and the other in the descending Sentinel-1 tracks, for the years 2014-2019, with maximum LOS velocities of 5 cm/y. 2. Decomposition of the LOS displacements to vertical and E-W horizontal components. 3. Recognition of linear trends of deformation (no acceleration nor deceleration). The paper is local and mostly technical, showing some interesting results, however, it does not make any attempt to discuss these results, their implications, or their contribution to our general understanding of sinkhole-related processes.

Reviewer 2, General comments: This manuscript applied InSAR to detect ground deformation related to salt extraction-caused sinkholes in Solotvyno (Ukraine). Both ascending and descending datasets from Sentinel-1 satellite were used to decompose horizontal and vertical displacement. Results found that the maximum LOS deformation is 5 cm/yr and the vertical deformation is much more dominant in the area. However, the aim of this paper is not completely clear: are the authors willing to prove the usefulness of InSAR applied to sinkhole deformation (focus on the methodology) or are they interested on the ground deformations detected on the salt mines (focus on the case studies)?

We agree with the reviewers for pointing out that the motivation of the paper is not fully clear. In the past decades satellite radar interferometry has become a widespread tool to detect subtle surface changes, like ground subsidence associated with sinkhole generation. The numerous studies available for the Dead Sea region clearly confirms that. With the advent of coordinated Earth observation, the near real time mapping of surface deformation processes become available. The recent paper by Nof et al. (2019) describes a semi-automatic early warning system that detects precursory subsidence before sinkhole collapse primary based on SAR dataset.

Our study area is not investigated as thoroughly as the Dead Sea region, but it is also severely affected by sudden sinkhole collapses. Collapse of subsurface caverns in the past resulted in dolines, temporally filled with brine and have a size of 150-230 m in diameter. Although today it can be handled as a local problem, it will definitely become a serious issue in the future as the water infiltration caused sinkhole development will propagate through the boundary of the mining area and endanger inhabited areas. Some parts of the city have already been evacuated. Besides the economic losses, the ecologic impact of migrating salt water into underground fresh water system can be catastrophic, which can lead to a regional problem. Recognizing the situation, the European Commission devoted considerable funds to support risk reduction in the area.

The latest sinkhole collapse happened before the launch of the Sentinel-1 mission. Although the issue is well-known, no dedicated terrestrial monitoring network has been installed yet. Therefore, Sentinel-1 satellite interferometry seems to be the only opportunity to support the early identification of areas prone to sinkhole occurrence.

We also agree with the reviewers that a thorough discussion of the results is needed to improve the paper, providing more insight into the mechanisms responsible for sinkhole growth in the area. Although the observed deformation pattern is sparse (Reviewer 1 also noted this regarding the cumulative displacement profiles in comment 6) we tried to perform an inversion to get some information about the dislocation sources. This investigation will be incorporated into the revised version of the ms.

Source modeling

We modeled the deformation observed by InSAR in order to better understand the mechanisms responsible for the sinkhole growth, and constrain the location and depth of underground cavities which can result in sinkhole collapse in the future. The cavity deflation was modeled using rectangular dislocation sources (Okada, 1992; Segall, 2010) within a homogeneous and isotropic elastic half-space. We used a rectangular pressurized crack model, since deformations are presumably related to the destruction of abandoned mines. Despite their simplicity and the inherited approximations, analytical formulations are convenient to model and explain deformation patterns described by a few model parameters. The elasticity assumption implies that the half-space obeys Hooke's law, therefore displacements are considered infinitely small compared to the characteristic size of source dimensions (Lisowski, 2007). The observed gradual subsidence also supports the assumption of pure elastic deformation.

Unfortunately, no reliable information is available on the exact position, extension, orientation and depth of the mining underground. The estimated depth of underground mines varies between 50 m to 400 m, from the center to the perimeter of the mining area. The approximate location of the mines was estimated based on the available maps. We fit simple Okada rectangular dislocation models to the InSAR data using a grid-search method to estimate the initial model parameters. These were refined in a second step based on a Bayesian inversion.

Forward modeling

The coarse estimation of model parameters was accomplished by forward modeling varying source model parameters on a predefined interval. The parameter space of the dislocation models was constrained based on the rough location, geometry and orientation of underground mines available on maps as well as the approximate depth of salt layer. Lack of coherence, either due to change in ground cover or high rate of deformation, does not allow to retrieve the entire deformation pattern associated with sinkhole evolution. Therefore, cumulative deformations from ascending and descending satellite passes covering the same time period, were utilized simultaneously to increase the reliability of source model

parameter estimation. The lack of deformation signal around the center of the area of interest makes it difficult to identify the number of source models required to explain the subsidence pattern. We made an exhaustive search for the best-fitting models using the misfit function $\delta = \left[\sum_{i=1}^{N}\sum_{j=1}^{M}\left(d_i - d_{i,m_j}\right)^2/N\right]^{1/2}$, where N is the total number of measurement points, M is the number of source models, d_i is the observed cumulative surface deformation and d_{i,m_j} is the modeled deformation from the j[th] source model projected onto the satellite LoS. Our results suggest a quad-source configuration of subsurface cavities, the model parameters are provided in Tabl. 1.

Source parameter estimation based on Bayesian inversion

To refine the source parameters and estimate associated uncertainties we performed a Bayesian probabilistic inversion (Bagnardi & Hooper, 2018). We modified the open-source GBIS (Geodetic Bayesian Inversion Software, http://comet.nerc.ac.uk/gbis/) code to handle custom source models of multiple rectangular dislocations. We also jointly inverted the cumulative ascending and descending InSAR data to determine deformation source parameters, i.e. horizontal dimensions and horizontal coordinates of rectangular source, depth of dislocation, strike angle of horizontal edge with respect to the North and opening of model (related to volume change), for every models in a single run. Within a Bayesian inversion approach the characterization of posterior probability density functions (PDFs) of source model parameters are accomplished by taking into account uncertainties in the data. The optimal set of source parameters can be extracted from the posterior PDF by finding the maximum a posteriori probability solution. The PDFs of source model parameters are determined from the likelihood function of the residuals between the observations and the model prediction weighted with the inverse of the variance-covariance matrix of the observations. The Bayesian inversion approach requires to quantify errors in the data, which are assumed to be multivariate Gaussian with zero mean and covariance matrix. For multiple independent data sets, the likelihood function can be formulated as the product of the likelihoods of the individual data sets. To increase the numerical efficiency, the GBIS inversion algorithm samples the posterior PDFs through a Markov chain Monte Carlo method, incorporating the Metropolis-Hastings algorithm, with automatic step size selection. For more details we refer to Bagnardi & Hooper (2018).

Noise covariance of individual interferograms has been well studied, the main error sources are the noise caused by the temporally correlated phase decorrelation and the spatially correlated atmospheric phase delay. Since InSAR observations are inherently relative, the additive phase delays make the accuracy of measurements strongly dependent on the distance. There have been several endeavors to provide an error analysis of TS (Time Series) InSAR output (see e.g. Agram & Simons, 2015; Cao et al., 2018 and references therein), however, we followed the method of Parizzi et al. (2020) and estimated the variance-covariance matrix of InSAR data sets experimentally. As Parizzi et al. (2020) points out, short time separated interferograms (supported by Sentinel-1 mission with multi-baseline analysis) are much more dominated by atmospheric propagation delay rather than phase variation due to deformation. After atmospheric phase correction the interferometric

measurement error is practically the residual atmospheric phase delay, as short time separated interferograms can be considered deformation-free. The mean variograms of the residual atmospheric phase shows a stationary behavior and can be approximated by a covariance function. Since both deformation and average velocity are related to the phase by a scale factor, the error estimates can be simply computed. We used an exponential covariance model fitted to the data to determine the variance-covariance matrix of deformation in the Bayesian inversion. For both the ascending and descending data sets similar models were obtained with a moderate range values of 2.4 and 2.2 km for the ascending and descending datasets respectively.

Best-fit model parameters obtained from the forward modeling were utilized as starting values for the Bayesian parameter estimation. During the inversion the parameters were allowed to vary within reasonable limits taking into account the geological constrains and information of the mining activity. The optimal model parameters are summarized in Tabl. 1., coordinates are given in a local rectangular coordinate system. Our final model assumes four rectangular-shaped subsurface cavities, developed in the salt layer. One source with a rectangular dislocation (model #1) of size 24.1 m × 64 m is located above the eastern edge of working panels of mine №9 at an estimated depth of 199.7 m. This mine was closed in 2008 due to water inrush. The moderate value of volume change suggests that this depression is an early stage of sinkhole development. The second source model (model #2) lies approximately 400 m southwest far from the first one and has a horizontal dimension of 63.5 m × 187.8 m, the required height change explaining the deformation pattern is -1.2 m. The elongated shape in roughly North-South direction of the source model is in agreement with the subsurface mining activity. Between the main corridors of mines №9 and №10 long working panels were cut with varying length between a few tens to a few hundreds of meters. The third dislocation model (model #3) is located in the western periphery of the area affected by deformations. The model is roughly symmetric with a horizontal side length about 80 m and located at a depth of 273.1 m. There are several shallow mines (numbered by 1 to 5 on Fig. 5. in the ms.) there, established around the 18-19th century. These were completely destroyed as the numerous, small-scale dolines filled with brine indicate on the surface. The source model parameters suggest that the inverse modeling tried to find a global solution for the observed subsidence pattern. However, a single source is unable to sufficiently explain the complex deformation pattern, a number of near-surface, small-scale voids, related to salt dissolution are needed as well. The fourth source model (model #4) is located beneath the working panels of mine №8, where heavy subsidence occurred around 2010, which resulted in the formation of the twin lakes. The depth of the model is about 296 m, the horizontal extension of the model is 72.3 m × 82.1 m. The estimated opening equals to approximately an 18,000 m^3 volume change. Taking into account the horizontal extension of the existing surface depressions of the nearby twin lakes, 15,000 and 17,000 m^2 respectively, our modeling results seem reasonable. The question whether a new doline will form and will merge with the existing two in the future or the boundary of the area affected by subsidence will expand toward south, requires further observations besides radar interferometry.

Regarding the quantitative analysis of the inversion results Figs. 1. and 2. shows the LoS deformation determined from the best-fitting quad-configuration source model, the Sentinel-1 cumulative LoS deformations as well as the difference between the observed and

modeled values, for both the ascending and descending passes respectively. It can be assessed that the main features of the subsidence pattern on the northern and southern periphery are reasonably well captured by the source models. However, the modeled deformation on the western part of the area does not fit to the observations, especially when comparing to the ascending data set, where modeled deformation overestimates the observed ones. As it was mentioned, under this area the salt layer upwells close to the surface and many small dropout doline have already formed and a single source model cannot adequately explain the surface deformation pattern.

Apart from larger discrepancies at some individual points the modeled deformation pattern fit well to the observed ones. However, it has to keep in mind when evaluating the inversion performance that it wasn't possible to properly sample the deformation pattern with InSAR, only the margins of the area was mapped adequately. Due to the sparse InSAR observation distribution in the middle of the area, we could not fit a proper source model there, which can be seen immediately when inspecting the modeled and observed deformations along selected profiles given on Fig. 3. Regarding the ascending data set, the same North-South oriented profile was used to check the model fit to InSAR observations as shown Fig. 10. (in the original ms.) to check the subsidence evolution in time. In the northern part (starting from point A to appr. 200 m) of the cross-section the source models are capable to explain reasonably well the observed deformation. The misfit of the modeled deformation is characterized by a standard deviation (std.) of ± 0.49 cm. However, for the second half of the investigated profile, between 200 and 800 m, the modeled deformation differs significantly from the observed ones. The reason for the large discrepancies in the middle of the cross-section comes from that, that it was not possible to find a proper source model based on the very scarce InSAR observations in the center of the area. On the southern edge of the cross-section (between 700 and 800 m) the applied single source model is not capable to resolve the observed deformation. Probably the InSAR derived deformations reflect the effect of more than a one subsurface cavern. The bottom figure of Fig. 3. shows the observed and modelled deformations on a roughly east-westward cross section (the location of the section is the same as for Fig. 11. in the original ms.). Modeled deformation shows a reasonably sufficient fit to the InSAR deformations. The misfit of the model is characterized by a ± 1.87 cm std. The magnitude of the observed deformation is adequately described by the model, however, the location of extremities is a slightly miss-estimated. The profile crosses the area in the North, where model #1 and model #2 is located. The effect of the two source models can be separated on the modeled deformations. Of course, the fine details revealed by InSAR observations cannot be reproduced by analytical modeling. Despite of the simple formulas, analytical models can produce reasonable first-order results of the subsurface processes. However, the possible interaction between the sources were not considered. As Pascal et al. (2013) points out, superposition of analytical models requires attention for adjacent models.

Reviewer 1, specific comment 1. The geographical and geological background is far too long and detailed and is mostly irrelevant to the scope of the paper. The background sentences in the introduction are sufficient to understand the setting.

Reviewer 2, specific comment 1. The authors talked a lot about geological settings in Section 2 “Geographical and geological background”, but it looks not related to your discussions later in the paper. The same problem as in Section 3. Could you relate your deformation results to the geological settings and mining activities? Maybe you can add a section in discussion to talk about the relationship between deformation and geological setting/ mining activities.

We agree with the reviewers that the given geological background is too lengthy in the present form. Our aim was to summarize the information available for the region, since most of the papers, textbook and maps are difficult to acquire and mostly written using the Cyrillic alphabet. We will shorten this section in the revised version of the ms. and add the results of the analytical source modeling to link the surface processes with geology and past mining activity.

Reviewer 1, specific comment 2. Materials and methods: lines 153-169 and 190-199 are introductory and background descriptions and should not appear in this section. Only lines 170-187 and 200-229 are relevant and should be combined with lines 53-62 to one section.

Reviewer 2, specific comment 2. In section 4 “Materials and methods”, the first paragraph (line 155-175) is not related to this section, you have to focus on your SAR datasets and what method you developed/used to process your SAR data. My suggestion is to simplify your section 2 and discuss more about your methodology. Describe more about what software you used to process Sentinel-1 data, how do you deal with coherent pixel selection, or maybe how to mitigate atmospheric delay.

We thank the referees this remark. In the revised ms. we will merge the suggested paragraphs for the introduction to Material and methods.

We also will include more details on Sentinel-1 processing in Section 4.2 as follows (from line 221., original text given in black).

The interferograms were generated using the Gamma software (Wegmüller et al., 2016). We considered pairs of four consecutive SAR scenes to include redundancy in the interferogram network, which facilitates reduction of errors. We utilized both phase-stable single scatterers (PS) as well as distributed targets (DS), which ensures long-term coherence. The initial set of PS candidates was selected based on the high temporal stability of the backscattering as well as the low spectral diversity. For the DS scatterers we used multilooking with a factor of 5 x 1 (5 samples in range and 1 in azimuth) to increase signal to noise ratio but keeping in mind the spatial extent of the sinkholes. Distributed targets resulted in a 15 m x 15 m pixel size in the slant range, which enables to detect localized

deformation caused by surface depression. The flat-earth phase and topographic phase were removed from the interferograms. In the multi-baseline approach interferograms were unwrapped in space first, finding the unambiguous phase values. The phase unwrapping was accomplished in an iterative way with quality control, keeping those PS and DS pixels for the next step, which satisfy the phase model with reasonably small (< 1 rad) residuals. A two-dimensional phase model involving height corrections relative to the reference model (SRTM heights mapped to radar coordinates) and linear deformation rate was chosen. The residual phase consists of non-linear deformation phase, atmospheric propagation delay, error in the height correction estimates and other noise terms. The spatially correlated, low-frequency part of the residual phase was separated by spatial filtering from the residual phase, since unwrapping residual phase of point differential interferograms is much simpler than unwrapping the original point differential interferograms. The whole process was iterated starting from dividing the area into patches, where the linear phase model approximation was suitable. Using a multi-reference stack based on consecutive SAR scenes, the deformation phase can be kept as small as possible. With the constant refinement of the phase model a single regression was applied on the whole area. The main output of the regression analysis was the unwrapped phase. The various phase terms were summed up and then the unwrapped phases were connected in time and inverted to deformations using a least squares approach minimizing the sum of the square weighted residual phases (Berardino, Fornaro, Lanari, & Sansosti, 2002; Wegmüller et al., 2016). The atmospheric phase and non-uniform deformation phase are present in the time series of unwrapped phases. To discriminate the two, we identified highly deforming areas and excluded those phase values to estimate atmospheric propagation delay. Atmospheric phases were determined as a combination of height dependent atmospheric delay plus the long-wavelength component of the SBAS inverted residual phase. We used a low-pass filter with characteristic length of 5 km. Long-wavelength (> 5 km) non-linear deformation was mapped into atmospheric correction. However, the area affected by subsidence is rather compact so we expect no long-wavelength non-uniform motion.

Reviewer 2, specific comment 3. The description of decomposition method in Section 5.2 should move to the section “Methods”. And in this section, you just need to discuss the decomposition results.

Thank you for the suggestion, we will move the paragraph describing LoS decomposition to Sec. 4. in the revised version of the ms.

Reviewer 1, specific comment 3. The authors present ascending and descending data and claim (line 254) that the “average (descending) deformation rate shows similar pattern as for the ascending pass. This suggests that the deformation consists mostly of vertical component.”. This declaration has not been proved in any way, for example, by a graph comparing all ascending vs descending LOS velocities. Furthermore, similar patterns are not enough to prove that claim, the values should also be close (albeit moderated by the incidence angle). This should be shown.

Reviewer 1, specific comment 5. The vertical velocities are about twice in magnitude (max 40 mm/y) compared to the horizontal velocities (max 20 mm/y). This means that deformation does not consist mostly of vertical deformation and that the horizontal movements should be considered and explained. Furthermore, Fig. 14 and lines 291-292 show that "The northern part of the deforming area clearly shows a westward displacement, whereas its southern part shows displacement towards the east". This means horizontal movements away from the subsidence centre (the sinkhole), which is counterintuitive, and should be explained and/or discussed.

We agree with the reviewer; the observed deformations must be explained in a coherent way, thanks for the inspiring comment. Considering a pure elastic model, the sketch beneath (please see the supplementary file) shows that the evolution of a depression means deformation not only with vertical component but horizontal as well. The farther a point from the center, the more pronounced is the horizontal deformation, which direction points away from the center of the subsidence bowl. Due to the side looking radar geometry, the observed horizontal deformation is not symmetric. However, asymmetry can also be caused by change in the material property (change in geology).

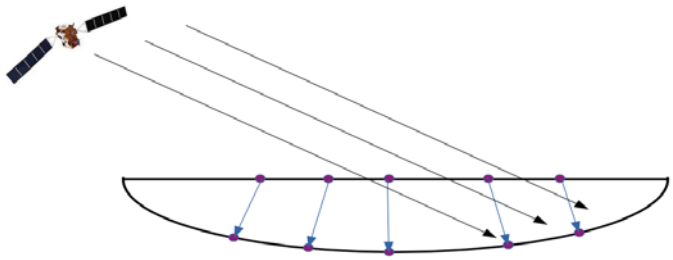

Reviewer 1, specific comment 4. The equation relating LOS to vertical and horizontal components should also include the heading angle between the track and the north.

Reviewer 2, specific comment 4. The equation of decomposition is wrong, the heading angle is missing. please refer to (Fuhrmann & Garthwaite, 2019).

Thank you for the reviewers to point out this issue. Since the North-South deformations are neglected in the decomposition, the azimuth enters only in the East-West term with the factor, cosine of the heading. Taking into account the heading values for S1, this term is about ±0.96 (depending on pass direction), therefore it was neglected. We acknowledge that equation of decomposition can be misleading in the present form, therefore, we will include the original, full 3D expression in the revised version of the ms. with proper citation.

Reviewer 1, specific comment 6. Figures 10 shows a cross sections over an area that is highly incoherent, while the lines are continuous from side to side. The authors should explain how this section was made and make it clear where are the true points and where are the lines based on interpolation.

We agree with the reviewer that it must be emphasized in the ms. that the LoS deformation profiles were constructed by interpolation. We applied a natural neighbor interpolation method based on the points satisfying some distance criteria (< 50 m) around the location of the profile. Therefore, Figs. 10. and 11. show much more the gradual deformation of a zone instead of the single profile. That's the reason we did not mark the location of true points on the deformation curves. This information will be added to the revised ms.
Location of cross-sections was selected to get information in roughly perpendicular directions of the area, it was chosen by visual inspection of point distribution.

Reviewer 1, specific comment 7. Line 183-184: "separation of total line-of-sight (LOS) deformation into east-west and vertical components which can help to understand the mechanism of sinkhole collapse and the progress of underground processes". The authors do not show anywhere later in the paper any insight or discussion regarding the mechanism of sinkhole collapse and progress of underground processes. So what is the motivation for this separation to vertical and horizontal components?

The separation of LoS deformation into vertical and horizontal components involves some spatial averaging to resample both datasets to a common grid, which has a smoothing effect. This can help to suppress possible outliers in one hand, on the other hand it is much easier to interpret horizontal and vertical deformations compared to LoS measurements. We agree with the reviewer, that the interpretation was not satisfactory. To constrain the underground processes, we conducted an analytical modeling described at the beginning of authors' responses.

Reviewer 1, specific comment 8. Lines 257-259: can the authors please explain the large difference between the ascending and descending velocities in the "landslide" area?

We did not investigate deformation pattern related to the landslide in the original ms., since we focused mining-related displacements, which can help the early identification of sinkhole prone areas.

Based on the relief (represented by SRTM model) and some assumptions about the nature of displacement related to landslide, we can conclude the following. Since this investigation is not part of the ms., the figs referred in the text can be found in the supplementary pdf material.

We take the assumption that the direction of motion is along the local direction of steepest descent, which is shown by the surface gradient vector. This condition is routinely applied not only in landslide mapping applications, but also in investigations related to glacier displacement mapping. The horizontal orientation of the gradient vector in the landslide area varies between -1.8 and -2.2 radian (-103°-126°), where angles are measured relative to the East and increases towards to the North. Therefore, the slope is assumed to move towards south with a slight westward motion (see first fig). The magnitude of the gradient vector is shown on the second figure, it is about 22-25%, which suggests a moderately steep slope. Assuming that the vertical deformation is more pronounced than the horizontal (westward) motion, which can be plausible based on the gradient vector, the apparent deformation in the LoS direction for the descending pass is larger (see the sketch on the

third fig.), that is the reason for the difference. [The incidence angles are 41.4° and 36.3°, for the ascending and descending passes respectively (see Tabl. 2. of the original ms.).]

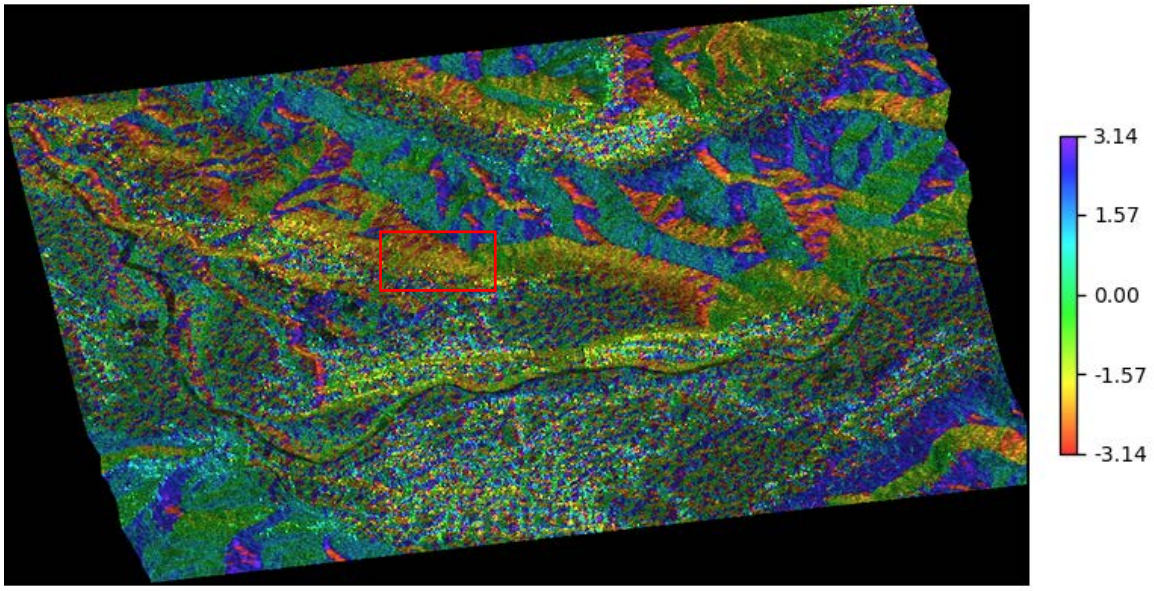

Orientation angle of SRTM gradient vector (values are in radian relative to East, North is π/2, South is –π/2), landslide area is marked by the red box.

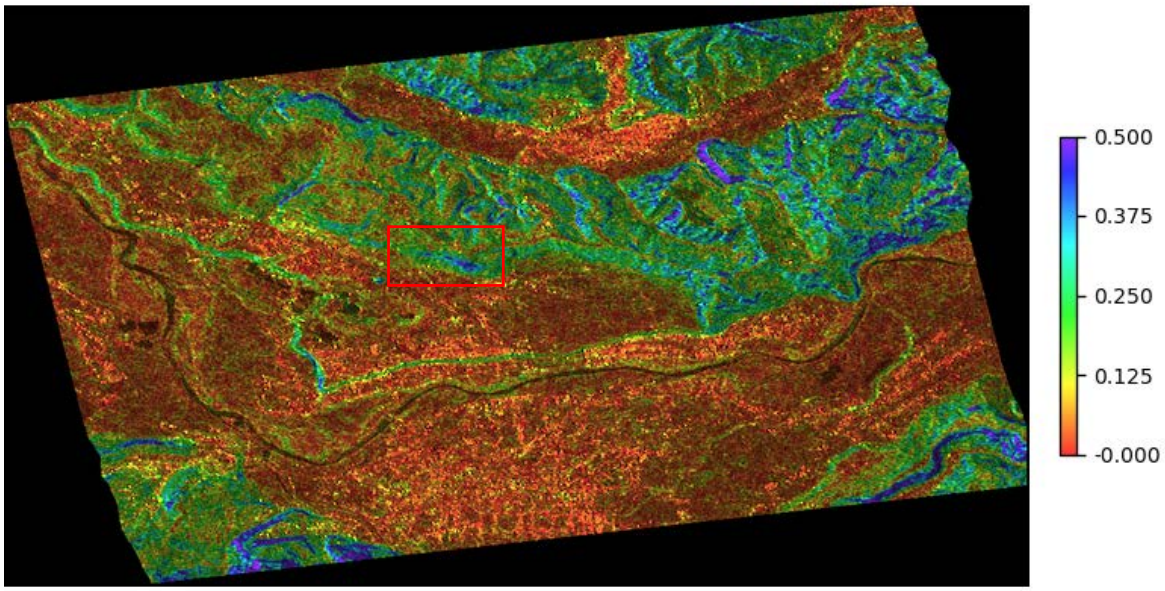

Normalized magnitude of the SRTM gradient vector.

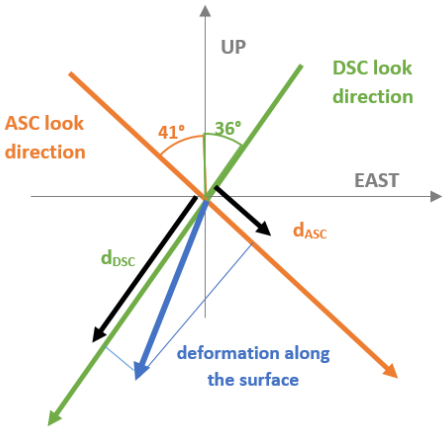

Reviewer 1, specific comment 9. Lines 261-264: The description of the two sides of the bowl is poorly supported by the figure.

Thanks for the comment, we added Fig. 3. based on source modelling to support the discussion.

Reviewer 1, specific comments 10. Lines 305-306: “guaranties to maintain coherence” – coherence is definitely not maintained in the central area.

We agree with the reviewer’s remark. It will be emphasized in the revised version of the ms. that the parameters of the Sentinel-1 mission, i.e. short revisit time, orbit positioning control, help to maintain coherence in general; however, any change in the surface backscatter properties can lead to coherence loss.

Reviewer 2, specific comment 1. The authors talked a lot about geological settings in Section 2 “Geographical and geological background”, but it looks not related to your discussions later in the paper. The same problem as in Section 3. Could you relate your deformation results to the geological settings and mining activities? Maybe you can add a section in discussion to talk about the relationship between deformation and geological setting/ mining activities.

We will add a section devoted to analytical modeling to explain the mechanism of sinkhole formation and its relation to mining activity in the area.

Reviewer 2, specific comment 5. I think your discussion is not enough, could you please talk about how the deformation results relate to the geological settings you described in Section 2.

We agree with the reviewer, the results of InSAR analysis is not coupled to the geological setting of the area, thank you for the comment. We will add a source modeling analysis, described above, to find a linkage between deformation evolution and geological setting and explain the subsurface processes.

Reviewer 1, technical corrections 1. The paper requires Language and grammar editing. Lots of sentences lack commas (,) to separate between parts of the sentence. Citation of previous studies should not be in brackets when they are the subject of the sentence. For example, line 143: (Gaidin, 2008) has already drew attention to: : :.., should be: Gaidin (2008) has already: : :.. This type of error appears many times in the paper. 2. Line 115: change horizontal extension to areal extent 3. Line 256: what is MT-InSAR? Fig. 7 is like 6 but descending

Reviewer 2, technical corrections: 1. Line 307, please check the citation format (Velasco et al.,
2017). And some of the same problems across the whole manuscript. 2. Line 221, Small Baseline Subset, SBAS -> Small Baseline Subset (SBAS) 3. Line 203, 1' resolution SRTM, is it 1 arc second?

Thank you for your comments. We will thoroughly check the English of the ms.

Regarding citations: We used the Mendeley Citation plugin (https://www.mendeley.com/guides/using-citation-editor) for MS Word. It is a rather convenient tool for generating references, citations and bibliographies. We will check and adjust manually the citation format where necessary in the revised ms.

The 1' resolution SRTM was released by USGS, we will add a proper reference in the revised ms, as:
Shuttle Radar Topography Mission 1 Arc-Second Global (Digital Object Identifier (DOI) number: /10.5066/F7PR7TFT

MT-InSAR stands for Multi-Temporal InSAR analysis, which is also called TS-InSAR (Time-Series InSAR) in the literature.

References

Agram, P. S., & Simons, M. (2015). Journal of Geophysical Research : Solid Earth A noise model for InSAR time series. *Journal of Geophysical Research : Solid Earth*, (May 2014), 1–20. https://doi.org/10.1002/2014JB011271.1.

Bagnardi, M., & Hooper, A. (2018). Inversion of Surface Deformation Data for Rapid Estimates of Source Parameters and Uncertainties: A Bayesian Approach. *Geochemistry, Geophysics, Geosystems*, *19*(7), 2194–2211. https://doi.org/10.1029/2018GC007585

Berardino, P., Fornaro, G., Lanari, R., & Sansosti, E. (2002). A new algorithm for surface deformation monitoring based on small baseline differential SAR interferograms. *IEEE Transactions on Geoscience and Remote Sensing*, *40*(11), 2375–2383. https://doi.org/10.1109/TGRS.2002.803792

Cao, Y., Li, Z., Wei, J., Hu, J., Duan, M., & Feng, G. (2018). Stochastic modeling for time series InSAR : with emphasis on atmospheric effects. *Journal of Geodesy*, *92*(2), 185–204. https://doi.org/10.1007/s00190-017-1055-5

Lisowski, M. (2007). Analytical volcano deformation source models. In *Volcano Deformation* (pp. 279–304). https://doi.org/10.1007/978-3-540-49302-0_8

Nof, R. N., Abelson, M., Raz, E., Magen, Y., Atzori, S., Salvi, S., & Baer, G. (2019). SAR Interferometry for Sinkhole Early Warning and Susceptibility Assessment along the Dead Sea, Israel. *Remote Sensing*, *11*(1), 89. https://doi.org/10.3390/rs11010089

Okada, Y. (1992). Internal deformation due to shear and tensile faults in a half-space. *Bulletin - Seismological Society of America*, *82*(2), 1018–1040.

Parizzi, A., Gonzalez, F. R., & Brcic, R. (2020). A covariance-based approach to merging InSAR and GNSS displacement rate measurements. *Remote Sensing*, *12*(2). https://doi.org/10.3390/rs12020300

Pascal, K., Neuberg, J., & Rivalta, E. (2013). On precisely modelling surface deformation due to interacting magma chambers and dykes. *Geophysical Journal International*, *196*(1), 253–278. https://doi.org/10.1093/gji/ggt343

SEGALL, P. (2010). *Earthquake and Volcano Deformation* (STU-Stud). Retrieved from http://www.jstor.org/stable/j.ctt7sg19

Wegmüller, U., Werner, C., Strozzi, T., Wiesmann, A., Frey, O., & Santoro, M. (2016). Sentinel-1 Support in the GAMMA Software. *Procedia Computer Science*, *100*, 1305–1312. https://doi.org/10.1016/j.procs.2016.09.246

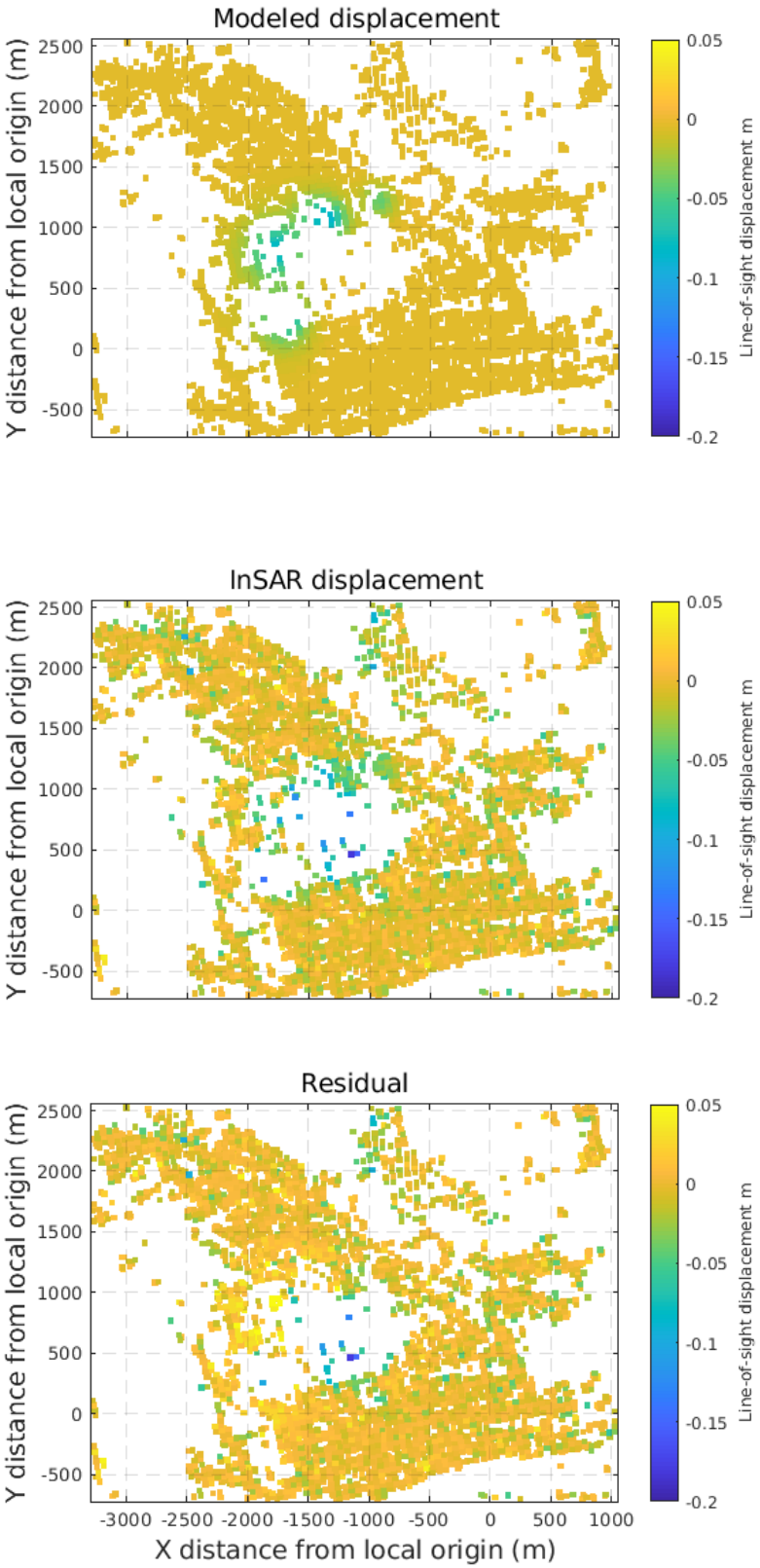

Fig. 1. Cumulative LoS deformation computed from the quad-configuration source model (top), deformation from the ascending Sentinel-1 observation (middle) and residuals after subtracting the best-fitting model

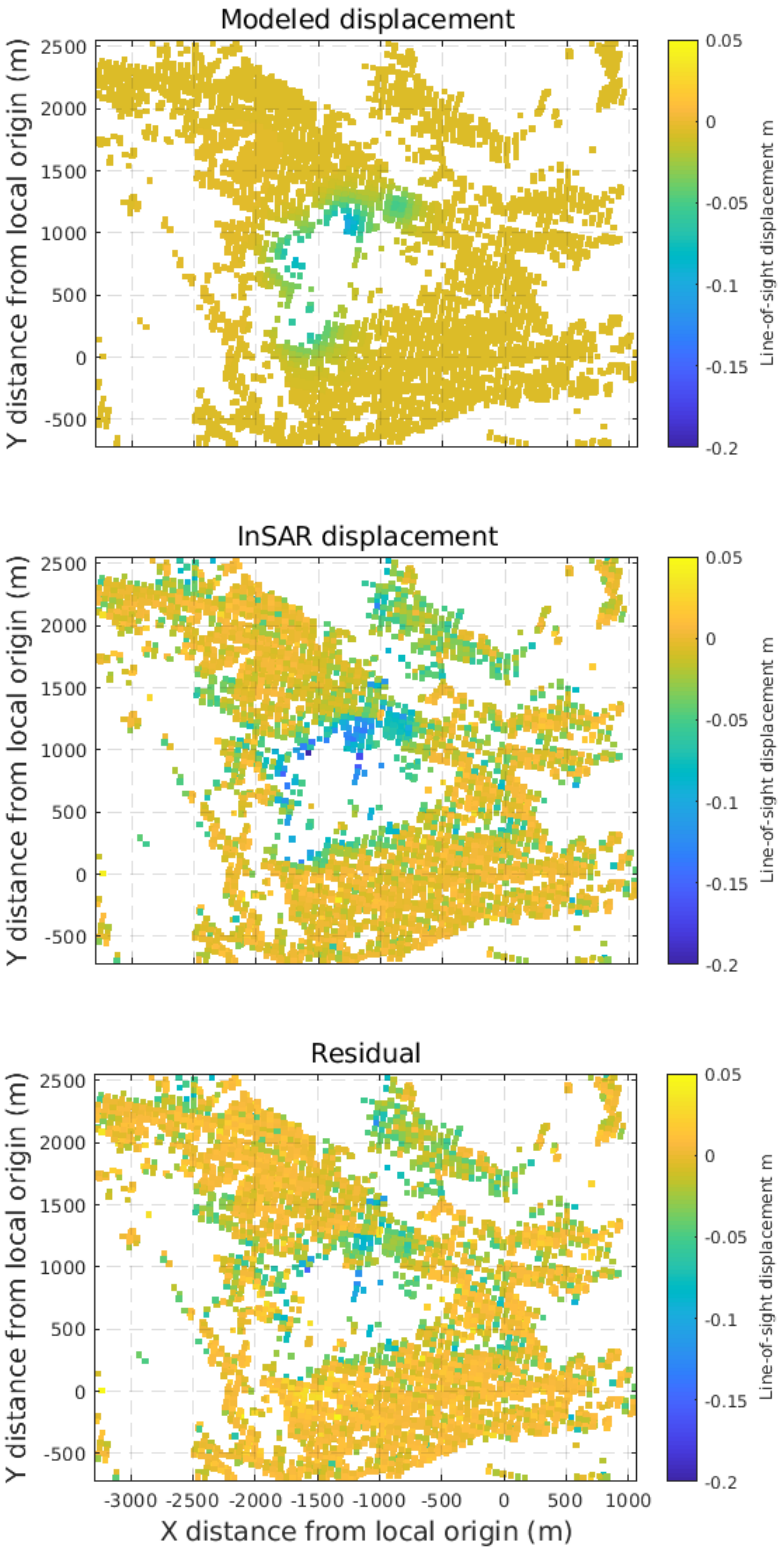

Fig. 2. Cumulative LoS deformation of the best-fitting model using four dislocation sources (top), deformation from the descending Sentinel-1 observation (middle) and residuals after subtracting the modeled displacement from the cumulative deformation

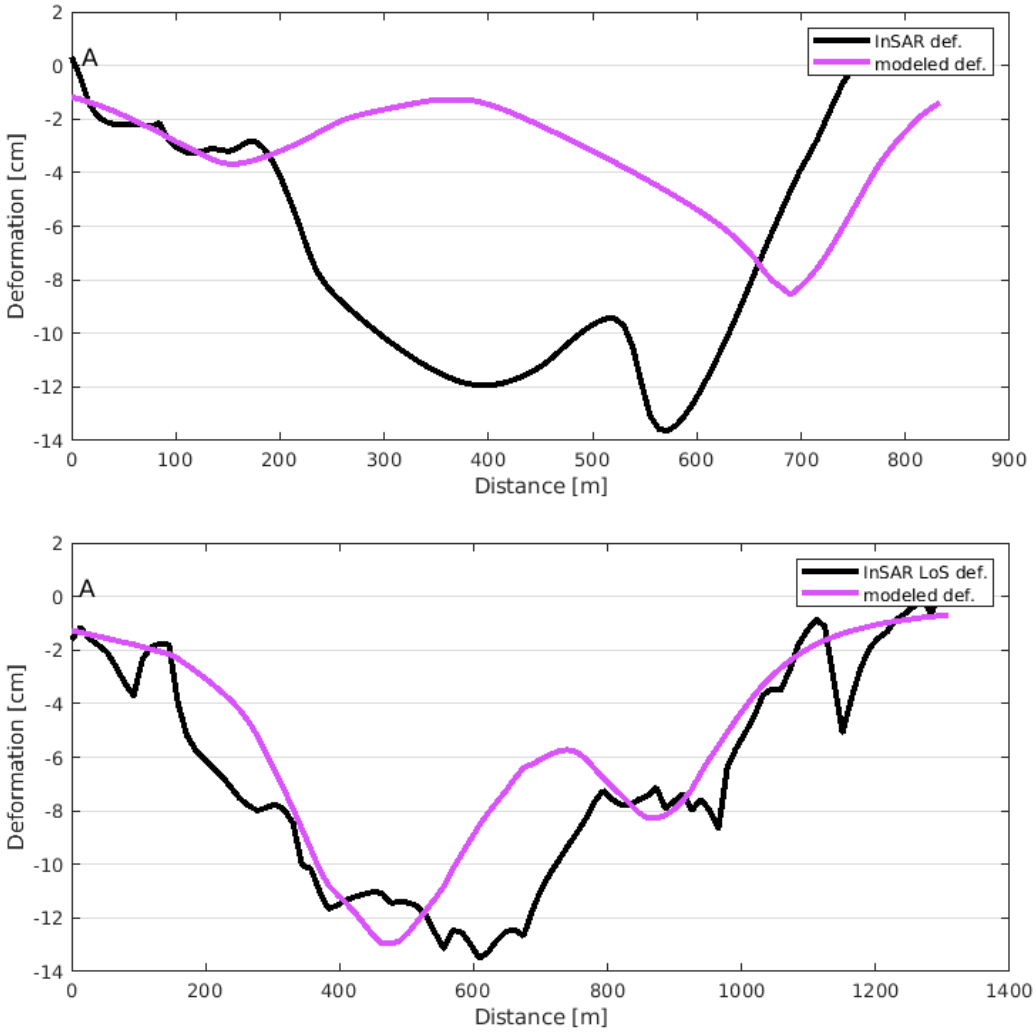

Fig. 3. Observed cumulative LoS and best-fitting model LoS deformations along selected profiles (given on Fig. 10. and 11. in the original ms.) for the ascending (top) and descending (bottom) passes.

Table 1. Analytical model parameters used in the source modeling. “I” refers to initial, “R” to refined values; coordinates are given in local rectangular system, shown on Fig. 1.

	model #1		model #2		model #3		model #4	
	I	R	I	R	I	R	I	R
length [m]	36	24.1	72.5	63.5	80	78.2	80	72.3
width [m]	42	64.0	176	187.8	80	81.8	90	82.1
depth [m]	180	199.7	222	231.9	280	273.1	295	295.9
strike angle [deg]	5	12.8	21.5	19.1	22	18.7	21	17.1
X center [m]	-870	-880.3	-1195	-1259.1	-1600	-1630.8	-1700	-1700.5
Y center [m]	1160	1195.8	956	1029.6	230	224.9	810	793.1
opening [m]	-3.2	-2.8	-1.4	-1.2	-3.9	-2.3	-3.8	-3.1